Int. J. Heat Mass Transfer. Vol. 34, No. 11, pp. 2899–2909, 1991
Printed in Great Britain

0017–9310/91 $3.00 + 0.00

Heat and mass transfer with a boundary layer flow past a flat plate of finite thickness

SHIGERU MORI, HIROSHI NAKAGAWA† and AKIRA TANIMOTO
Department of Chemistry and Chemical Engineering, Kanazawa University, Kanazawa 920, Japan

and

MIKIO SAKAKIBARA
Department of Applied Chemistry, Fukui University, Fukui 910, Japan

(*Received* 22 *March* 1990 *and in final form* 4 *December* 1990)

Abstract—Evaporation from a flat-plate surface to a laminar boundary layer flow past the plate is theoretically analyzed, taking into account the two-dimensional thermal conduction in the plate, with the convective thermal-boundary condition on the other plate surface. The thermal effect of the volatile liquid supply to the plate is neglected. Distributions of the interfacial temperature and the local Nusselt and Sherwood numbers are calculated for a parallel flow where both Prandtl and Schmidt numbers are equal to unity. The characteristics in heat and mass transfer are revealed to be significantly influenced by the temperature dependency of the vapor–liquid equilibrium, the magnitude of the latent heat of phase change, and the thermal conductance of the flat plate.

1. INTRODUCTION

IN ABLATION or perspiration cooling problems and heterogeneous chemical reaction problems, information on the interfacial temperature and concentration distributions is essential because the transfer characteristics are mainly determined by the temperature and concentration differences between the bulk flow and the interface. As a fundamental study for those problems, analyses of the conjugate thermal problem between convective heat transfer and thermal conduction in the neighboring flat plate wall are of great interest. In cases with chemical reaction, for instance, combustion problems might be too complicated to be dealt with analytically, taking account of the thermal conduction in the wall, because not only concentration and temperature dependence of the reaction rate but also transfers of various kinds of reactants and products make such problems more difficult to analyze even though the wall conduction is negligible [1].

For coupling of convective heat transfer in a boundary layer flow over a flat plate of finite thickness with two-dimensional thermal conduction in the plate, a leading study was presented in 1961 by Perelman [2] for a case with heat generation in the plate. He derived theoretical expressions for the interfacial temperature and the local Nusselt number. The investigation was extended to a case with a compressible gas flow by Luikov *et al.* [3]. They presented analytical solutions, taking into account the fluid viscosity dependent on the temperature. However, in both articles no numerical results were given. Later, a case with a flat plate of finite length was comprehensively analyzed in detail in ref. [4], by expanding the interfacial temperature $\theta(x)$ into a power series of $\sqrt{x}$ with unknown coefficients to be determined. The interfacial temperature and the local Nusselt number for cases with the first- and second-kind boundary conditions on the outer plate surface were calculated. It was found that the interfacial temperature is influenced markedly by the wall conduction when the plate is short and/or thick and its thermal conductivity is high in comparison with that of the fluid.

On the other hand, a one-dimensional approximation of the conduction process in a flat plate has been introduced, for example, by Luikov [5] and most recently by Pozzi and Lupo [6] for simplicity and practical uses or further theoretical extensions. The validity and the applicability of the simplification must be examined by detailed analyses including the axial thermal conduction.

In the present study, evaporation from a surface of a porous flat plate of finite thickness filled with a volatile liquid to a boundary layer flow is theoretically analyzed as an extension of the previous work [4], by combining the mass transfer with the conjugate heat transfer between the flow and the plate through the vapor–liquid equilibrium relationship. In the analysis, the two-dimensional thermal conduction in the plate is accounted for to clarify the axial conduction effect and the outside thermal condition is specified as the third kind. However, influence of the liquid flow in

† Present address: Tonen Chemical Corp., Ukishima-cho, Kawasaki 210, Japan.

NOMENCLATURE

a	coefficient in equation (12) [kg m^{-3} K^{-1}]
A	dimensionless coefficient, $a(T_\infty - T_h)/(C_t - C_\infty)$
b	constant in equation (12) [kg m^{-3}]
B	dimensionless constant, $(C_h - C_\infty)/(C_t - C_\infty)$
Bi	Biot number, $h\delta/k_w$
C	concentration [kg m^{-3}]
C^*	dimensionless concentration, $(C - C_\infty)/(C_t - C_\infty)$
C_h	saturated concentration at T_h [kg m^{-3}]
C_t	saturated concentration at T_∞ [kg m^{-3}]
D	diffusion coefficient [m^2 s^{-1}]
h	heat transfer coefficient between plate and ambient fluid [W m^{-2} K^{-1}]
H	dimensionless latent heat of vaporization, $\lambda(C_t - C_\infty)/\{\rho c_p(T_\infty - T_h)\}$
j	$(i-1)/2$
k	thermal conductivity [W m^{-1} K^{-1}]
L	plate length [m]
L^*	aspect ratio of plate, δ/L
m	index in equation (14), parameter relating to plate inclination
$M_j(\eta)$	normalized function defined in equation (47)
Nu_x	local Nusselt number, equation (61)
Pr	Prandtl number, ν/α
R_w	ratio of thermal conductances of plate and stream, $k_w L/(k_f \delta)$
Sc	Schmidt number, ν/D
Re_x	local Reynolds number, $u_\infty x/\nu$
Re_L	local Reynolds number at $x = L$, $u_\infty L/\nu$
Sh_x	local Sherwood number, equation (62)
T	temperature [K]
U	coefficient in equation (14) [m^{1-m} s^{-1}]
u	velocity component [m s^{-1}]
x	coordinate along flat plate [m]
x^*	dimensionless coordinate, x/L
y	coordinate perpendicular to plate [m]
y^*	dimensionless coordinate, y/L
$\hat{y}$	dimensionless coordinate, y/δ
$Y_j(\eta)$	normalized function defined in equation (42)
Z	$1 + C^*$.

Greek symbols

α	thermal diffusivity [m^2 s^{-1}]
β_i	coefficient in power series
δ	thickness of flat plate [m]
η	similarity variable, $(y/2)\{u_\infty/(\nu x)\}^{1/2}$
θ	dimensionless temperature, $(T - T_h)/(T_\infty - T_h)$
λ	latent heat of vaporization [J kg^{-1}]
ν	kinematic viscosity [m^2 s^{-1}]
ρ	fluid density [kg m^{-3}]
τ_i	coefficient in power series, to be determined
ϕ	dimensionless stream function, equation (20)
ψ	stream function, $(u_\infty \nu x)^{1/2}\phi(\eta)$.

Subscripts

f	boundary layer flow
h	ambient fluid
i	boundary layer–plate interface
w	plate
x	component in the x-direction
y	component in the y-direction
∞	outside of boundary layer.

the porous plate due to the liquid supply on heat transfer is neglected to simplify the problem. Distributions of interfacial temperature, the local Nusselt and local Sherwood numbers were calculated for a parallel-flow case where the Prandtl and the Schmidt numbers are equal to unity. The effects of wall conduction and the interaction of heat and mass transfer on them are discussed in detail and verified the validity of the traditional analogy concept between the heat and mass transfers.

2. THEORETICAL ANALYSIS

The problem analyzed in the present work is such that a gas of temperature T_∞, concentration C_∞ and velocity u_∞ passes under the laminar flow condition over a flat plate of thickness δ, length L and with an inclination angle $m\pi/(m+1)$ to the flow ($m = 0$ corresponds to a flow parallel to the plate and $m = 1$ to a stagnation flow). The plate is porous and completely filled with a volatile liquid, and the plate surface is covered with a very thin and stagnant liquid film. The heat and mass transfers through the front end of the plate are assumed to be negligibly small in comparison with that through the plate surface, similarly in the literature [2–4]. This is consistent with the boundary layer approximation of the Navier–Stokes equations. The trailing edge is connected with a semi-infinite insulated plate. The opposite surface of the plate is exposed to an ambient fluid stream of temperature T_h lower than that of the gas stream and the ambient convection is described by the heat transfer coefficient h.

Under such a situation, heat is transferred from the bulk flow to the interface through the developing boundary layer along the plate wall and the liquid vaporizes and diffuses from the liquid film on the plate surface to the free stream. The rates of heat and mass

transfers are not independent but conjugated with each other by the characteristic equilibrium relation, being different from that in simple heat or mass transfer problems. Therefore, the characteristics of heat transfer and mass transfer cannot be predicted easily from the solutions of simple heat or mass transfer problems. But it can be derived if the momentum and energy equations of the gas flow and the conduction equation of the plate wall are solved simultaneously under the conjugate boundary conditions describing the continuities of temperature and energy flux and the vapor–liquid equilibrium at the interface.

The present analysis is suitable for the following cases: (1) sublimation or ablation of a flat plate where a decrease in the plate thickness is relatively small; (2) perspiration cooling of a flat plate where liquid vaporizes only from the plate surface; (3) chemical reaction on the plate surface where mass transfer in the boundary layer flow is rate-controlling; (4) vaporization from a stagnant liquid film on a plate where a decrease in the film thickness and the thermal resistance of the film are comparatively small and negligible.

This model includes a special case with a constant temperature on the opposite wall surface, which is obtained as a limit case when h approaches infinity. The analyzed states of the bulk stream, the interface and the ambient temperature are shown in a temperature–concentration plane of Fig. 1. In the figure, C_t and C_h refer to the concentrations saturated at the bulk-stream temperature T_∞ and the ambient fluid temperature T_h, respectively.

The coordinate system used in the present analysis is such that the origin is at the leading edge, the abscissa x along the plate and the ordinate y normal to the plate surface.

To simplify the theoretical analysis, the following assumptions are introduced:

(1) gas is incompressible Newtonian fluid;

(2) all physical properties are constant, being independent of either temperature or concentration;

(3) bulk-stream velocity is described by equation (14) of the Falkner–Skan flow;

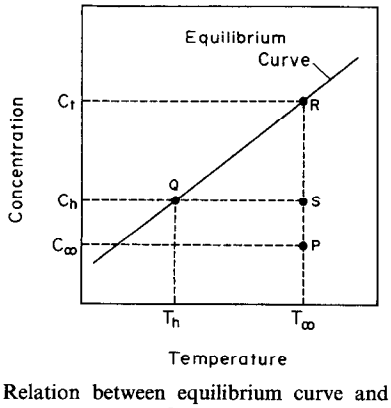

FIG. 1. Relation between equilibrium curve and driving forces.

(4) energy dissipation due to fluid viscosity is negligible;

(5) thermal conduction and mass diffusion in the x-direction in the fluid can be neglected in comparison with those in the y-direction;

(6) injection accompanied by vaporization has no influence on flow condition;

(7) gas at the interface is saturated at the interfacial temperature and its equilibrium relation can be expressed by a linear function of temperature.

2.1. *Governing equations*

The governing equations in momentum, heat and mass boundary layers can be formulated as follows for the two-dimensional steady-state problem.

2.1.1. *Fundamental equations for fluid flow.*

Equation of continuity

$$\frac{\partial u_x}{\partial x}+\frac{\partial u_y}{\partial y}=0 \tag{1}$$

and equation of momentum transfer in the x-direction

$$u_x\frac{\partial u_x}{\partial x}+u_y\frac{\partial u_x}{\partial y}=\nu\frac{\partial^2 u_x}{\partial y^2}+u_\infty\frac{\partial u_\infty}{\partial x} \tag{2}$$

with boundary conditions

$$\text{at } x=0, \quad u_x=u_\infty \tag{3}$$

$$\text{at } y=0, \quad u_x=u_y=0 \tag{4}$$

$$\text{at } y=\infty, \quad u_x=u_\infty. \tag{5}$$

Equation of energy transfer

$$u_x\frac{\partial T_f}{\partial x}+u_y\frac{\partial T_f}{\partial y}=\alpha\frac{\partial^2 T_f}{\partial y^2} \tag{6}$$

with boundary conditions

$$\text{at } x=0, \quad T_f=T_\infty \tag{7}$$

$$\text{at } y=0, \quad T_f=T_i(x) \tag{8}$$

$$\text{at } y=\infty, \quad T_f=T_\infty. \tag{9}$$

Equation of mass transfer

$$u_x\frac{\partial C}{\partial x}+u_y\frac{\partial C}{\partial y}=D\frac{\partial^2 C}{\partial y^2} \tag{10}$$

with boundary conditions

$$\text{at } x=0, \quad C=C_\infty \tag{11}$$

$$\text{at } y=0, \quad C=C_i(x)=aT_i(x)+b \tag{12}$$

$$\text{at } y=\infty, \quad C=C_\infty. \tag{13}$$

Bulk-stream velocity of Falkner–Skan flow

$$u_\infty=Ux^m. \tag{14}$$

2.1.2. *Fundamental equations for wall.*

Equation of wall heat conduction

$$\frac{\partial^2 T_w}{\partial x^2}+\frac{\partial^2 T_w}{\partial y^2}=0 \tag{15}$$

with boundary conditions

$$\text{at } x = 0 \text{ and } L, \quad \partial T_w/\partial x = 0 \tag{16}$$

$$\text{at } y = 0, \quad T_f = T_i(x) \tag{17}$$

$$\text{at } y = -\delta, \quad -k_w \frac{\partial T_w}{\partial y} = h(T_w - T_h). \tag{18}$$

In the above, equations (8) and (17) are the conjugation of the temperature continuity at the stream–wall interface, and equation (12) is that of heat and mass transfers through the equilibrium. The last conjugate relation is given as follows.

Conjugate boundary condition on energy flux

$$\text{at } y = 0, \quad -k_f \frac{\partial T_f}{\partial y} = -k_w \frac{\partial T_w}{\partial y} + \lambda D \frac{\partial C}{\partial y}. \tag{19}$$

2.1.3. *Normalization.* First, to rewrite the fundamental equations for the boundary layer flow, we introduce the following similarity variable and stream function:

$$\eta = \frac{y}{2}\left(\frac{u_\infty}{\nu x}\right)^{1/2}; \quad \psi = (u_\infty \nu x)^{1/2}\phi(\eta). \tag{20}$$

Second, to normalize the entire problem, dimensionless variables and parameters are defined as follows:

$$x^* = x/L; \quad y^* = y/L; \quad \hat{y} = y/\delta;$$

$$\theta = \frac{(T - T_h)}{(T_\infty - T_h)}; \quad C^* = \frac{(C - C_\infty)}{(C_i - C_\infty)};$$

$$Bi = h\delta/k_w; \quad R_w = (k_w L)/(k_f \delta); \quad L^* = \delta/L;$$

$$Pr = \nu/\alpha; \quad Sc = \nu/D;$$

$$H = \frac{\lambda(C_i - C_\infty)}{\rho c_p (T_\infty - T_h)}; \quad Re_L = \frac{u_\infty L}{\nu};$$

$$A = \frac{a(T_\infty - T_h)}{C_i - C_\infty} = \frac{C_i - C_h}{C_i - C_\infty}; \quad B = \frac{C_h - C_\infty}{C_i - C_\infty}.$$

On the basis of the previous assumption (7), and by referring to Fig. 1, it can be seen that parameter A is equal to the ratio of segment RS to segment RP and B is that of SP to RP. Accordingly B is dependent of A and can be expressed as $B = 1 - A$.

Thus all equations (1)–(19) are rewritten as follows.

Equation for stream function

$$\frac{d^3\phi}{d\eta^3} + (m+1)\phi\frac{d^2\phi}{d\eta^2} + 2m\left\{4 - \left(\frac{d\phi}{d\eta}\right)^2\right\} = 0 \tag{21}$$

with boundary conditions

$$\text{at } \eta = 0, \quad \phi = 0 \quad \text{and} \quad d\phi/d\eta = 0 \tag{22}$$

$$\text{at } \eta = \infty, \quad d\phi/d\eta = 2. \tag{23}$$

Energy equation for fluid stream

$$\frac{\partial^2\theta_f}{\partial\eta^2} + (m+1)\phi\, Pr\frac{\partial\theta_f}{\partial\eta} - 2x^*\phi'\, Pr\frac{\partial\theta_f}{\partial x^*} = 0 \tag{24}$$

with boundary conditions

$$\text{at } x^* = 0, \quad \theta_f = 1 \tag{25}$$

$$\text{at } \eta = 0, \quad \theta_f = \theta_i(x^*) \tag{26}$$

$$\text{at } \eta = \infty, \quad \theta_f = 1. \tag{27}$$

Mass transfer equation

$$\frac{\partial^2 C^*}{\partial\eta^2} + (m+1)\phi\, Sc\frac{\partial C^*}{\partial\eta} - 2x^*\phi'\, Sc\frac{\partial C^*}{\partial x^*} = 0 \tag{28}$$

with boundary conditions

$$\text{at } x^* = 0, \quad C^* = 0 \tag{29}$$

$$\text{at } \eta = 0, \quad C^* = C_i^*(x^*) = A\theta_i(x^*) + B \tag{30}$$

$$\text{at } \eta = \infty, \quad C^* = 0. \tag{31}$$

When a new variable $Z(x^*, \eta) = 1 + C^*$ is introduced, the above problem is rewritten as

$$\frac{\partial^2 Z}{\partial\eta^2} + (m+1)\phi\, Sc\frac{\partial Z}{\partial\eta} - 2x^*\phi'\, Sc\frac{\partial Z}{\partial x^*} = 0 \tag{32}$$

with boundary conditions

$$\text{at } x^* = 0, \quad Z = 1 \tag{33}$$

$$\text{at } \eta = 0, \quad Z = 1 + C_i^*(x^*) = A\theta_i(x^*) + B + 1 \tag{34}$$

$$\text{at } \eta = \infty, \quad Z = 1. \tag{35}$$

Consequently, the mass transfer equation and the boundary conditions are reduced to the same equations as those for the energy transfer, equations (24)–(27). In the above and hereafter the prime denotes differentiation with respect to η.

Energy equation for wall

$$L^{*2}\frac{\partial^2\theta_w}{\partial x^{*2}} + \frac{\partial^2\theta_w}{\partial\hat{y}^2} = 0 \tag{36}$$

with boundary conditions

$$\text{at } x^* = 0 \text{ and } 1, \quad \partial\theta_w/\partial x^* = 0 \tag{37}$$

$$\text{at } \hat{y} = 0 \quad \theta_w = \theta_i(x^*) \tag{38}$$

$$\text{at } \hat{y} = -1, \quad \partial\theta_w/\partial\hat{y} = -Bi\,\theta_w. \tag{39}$$

Conjugate boundary condition on energy flux at interface

$$-\left.\frac{\partial\theta_f}{\partial y^*}\right|_{y^*=0} = -R_w\left.\frac{\partial\theta_w}{\partial\hat{y}}\right|_{\hat{y}=0} + \left.\frac{H\,Pr}{Sc}\frac{\partial C^*}{\partial y^*}\right|_{y^*=0}. \tag{40}$$

2.2. *Solution procedure*

The momentum boundary layer problem, equations (21)–(23), is a two-point boundary value problem. Since it is hard to solve analytically, numerical analysis is required.

The solution of the energy equation is assumed to be in the following infinite series as in the previous work [4]:

$$\theta_f(x^*, \eta) = 1 + \theta_1(x^*, \eta) + \theta_2(x^*, \eta) + \theta_3(x^*, \eta) + \cdots + \theta_j(x^*, \eta) + \cdots. \tag{41}$$

Furthermore, we assume the dependency on x^* as follows:

$$\theta_f(x^*,\eta) = 1+\sum_{i=1}^{\infty}\tau_i x^{*j} Y_j(\eta) \tag{42}$$

where

$$j=(i-1)/2.$$

Then we obtain the following ordinary differential equation with respect to $Y_j(\eta)$:

$$\frac{d^2Y_j}{d\eta^2}+(m+1)\phi\, Pr\frac{dY_j}{d\eta}-2j\phi'\, Pr\, Y_j=0 \tag{43}$$

with boundary conditions

$$\text{at } \eta=0, \quad Y_j=1 \tag{44}$$

$$\text{at } \eta=\infty, \quad Y_j=0. \tag{45}$$

Consequently the interfacial temperature is represented by

$$\theta_i(x^*)=\theta_f(x^*,0)=1+\sum_{i=1}^{\infty}\tau_i x^{*j}. \tag{46}$$

On the other hand, the mass transfer problem is treated in a similar way, that is, we assume the following solution:

$$Z(x^*,\eta)=1+C^*(x^*,\eta)=1+\sum_{i=1}^{\infty}\beta_i x^{*j}M_j(\eta) \tag{47}$$

where

$$j=(i-1)/2.$$

Then the following ordinary differential equation with respect to $M_j(\eta)$ is obtained:

$$\frac{d^2M_j}{d\eta^2}+(m+1)\phi\, Sc\frac{dM_j}{d\eta}-2j\phi'\, Sc\, M_j=0 \tag{48}$$

with boundary conditions

$$\text{at } \eta=0, \quad M_j=1 \tag{49}$$

$$\text{at } \eta=\infty, \quad M_j=0. \tag{50}$$

Accordingly the interfacial concentration becomes

$$\text{at } \eta=0, \quad Z(x^*,0)=1+C_i^*(x^*)=1+\sum_{i=1}^{\infty}\beta_i x^{*j}. \tag{51}$$

At the interface, the equilibrium relation should be satisfied, thus

$$C_i^*(x^*)=A\theta_i(x^*)+B=B+A\left(1+\sum_{i=1}^{\infty}\tau_i x^{*j}\right). \tag{52}$$

Consequently values of β_i are combined with values of τ_i as

$$\beta_1=A(1+\tau_1)+B \quad \text{and} \quad \beta_i=A\tau_i. \tag{53}$$

Taking into account the linear dependency of the equilibrium at the interface, we have

$$\beta_1=1+A\tau_1. \tag{54}$$

The preceding two ordinary differential equations with respect to $Y_j(\eta)$ and $M_j(\eta)$ are of the same two-point boundary value problem with different parameter. These equations and $\phi(\eta)$ can be solved simultaneously by numerical integration.

On the contrary, the heat conduction equation for the wall can be solved analytically by applying the traditional technique of separation-of-variables

$$\theta_w(x^*,\hat{y})=\frac{1+Bi(1+\hat{y})}{1+Bi}\left(1+\sum_{i=1}^{\infty}\frac{2}{i+1}\tau_i\right)+2\sum_{n=1}^{\infty}\frac{n\pi L^*\cosh\{n\pi L^*(1+\hat{y})\}+Bi\sinh\{n\pi L^*(1+\hat{y})\}}{n\pi L^*\cosh(n\pi L^*)+Bi\sinh(n\pi L^*)}\times\cos(n\pi x^*)\left(\sum_{i=1}^{\infty}\tau_i\int_0^1\xi^{(i-1)/2}\cos(n\pi\xi)\,d\xi\right). \tag{55}$$

In these equations, the coefficients τ_i and β_i are unknown. These coefficients can be determined in the following way.

The conjugate boundary condition on the interfacial energy flux, equation (40), is modified to give the following two equations:

$$\int_0^1\left.\frac{\partial\theta_f}{\partial y^*}\right|_{y^*=0}dx^*-R_w\int_0^1\left.\frac{\partial\theta_w}{\partial\hat{y}}\right|_{\hat{y}=0}dx^*+\frac{H\,Pr}{Sc}\int_0^1\left.\frac{\partial C^*}{\partial y^*}\right|_{y^*=0}dx^*=0 \tag{56}$$

$$\int_0^1\left.\frac{\partial\theta_f}{\partial y^*}\right|_{y^*=0}\cos\{(N-1)\pi x^*\}\,dx^*-R_w\int_0^1\left.\frac{\partial\theta_w}{\partial\hat{y}}\right|_{\hat{y}=0}\cos\{(N-1)\pi x^*\}\,dx^*+\frac{H\,Pr}{Sc}\int_0^1\left.\frac{\partial C^*}{\partial y^*}\right|_{y^*=0}\cos\{(N-1)\pi x^*\}\,dx^*=0 \tag{57}$$

where

$$N=2,3,4,\ldots.$$

The dimensionless temperature gradient at the interface on the fluid side is calculated from equation (42) as

$$\left.\frac{\partial\theta_f}{\partial y^*}\right|_{y^*=0}=\left.\frac{\partial\theta_f}{\partial\eta}\frac{\partial\eta}{\partial y^*}\right|_{\eta=0}=\frac{\sqrt{(Re_L)}}{2}\left(\sum_{i=1}^{\infty}\tau_i x^{*(i-2)/2}Y_j'(0)\right) \tag{58}$$

and that at the plate-side interface from equation (55) as

$$\left.\frac{\partial\theta_w}{\partial\hat{y}}\right|_{\hat{y}=0} = \frac{Bi}{1+Bi}\left(1+\sum_{i=1}^{\infty}\frac{2}{i+1}\tau_i\right) + 2\sum_{n=1}^{\infty}\frac{n\pi L^*\tanh(n\pi L^*)+Bi}{n\pi L^*+Bi\tanh(n\pi L^*)} \times n\pi L^*\cos(n\pi x^*)\left(\sum_{i=1}^{\infty}\tau_i\int_0^1\xi^{(i-1)/2}\cos(n\pi\xi)\,d\xi\right). \quad (59)$$

Similarly the interfacial concentration gradient is also derived from equation (47) as follows:

$$\left.\frac{\partial C^*}{\partial y^*}\right|_{y^*=0} = \left.\frac{\partial C^*}{\partial\eta}\frac{\partial\eta}{\partial y^*}\right|_{\eta=0} = \frac{\sqrt{(Re_L)}}{2}\left(\sum_{i=1}^{\infty}\beta_i x^{*(i-2)/2}M_j'(0)\right). \quad (60)$$

After substituting equations (58)–(60) into equations (56) and (57), we obtain a set of simultaneous arithmetic equations with respect to values of τ_i. If the set of arithmetic equations is solved to determine the coefficients τ_i, the other coefficients β_i, the interfacial temperature gradients and the concentration gradient at the interface can be calculated from the values of τ_i.

The local Nusselt number and the local Sherwood number are defined as follows:

$$Nu_x = \frac{-\left.\frac{\partial\theta_f}{\partial y^*}\right|_{y^*=0}}{\theta_i(x^*)-1}x^* = -\frac{\sum_{i=1}^{\infty}\tau_i x^{*j}Y_j'(0)}{2\sum_{i=1}^{\infty}\tau_i x^{*j}}\sqrt{(Re_x)} \quad (61)$$

$$Sh_x = \frac{-\left.\frac{\partial C^*}{\partial y^*}\right|_{y^*=0}}{C_i^*(x^*)}x^* = -\frac{\sum_{i=1}^{\infty}\beta_i x^{*j}M_j'(0)}{2\left(1+A\sum_{i=1}^{\infty}\tau_i x^{*j}\right)}\sqrt{(Re_x)} \quad (62)$$

where

$$Re_x = u_\infty x/\nu, \quad j = (i-1)/2.$$

According to classical investigations on heat transfer with a laminar boundary layer flow over a flat plate, the local Nusselt number is given for a constant-wall-temperature case [7] as

$$Nu_x = 0.332\sqrt{(Re_x)}Pr^{1/3} \quad (63)$$

and for the case with constant interfacial heat flux [8] as

$$Nu_x = 0.453\sqrt{(Re_x)}Pr^{1/3}. \quad (64)$$

3. NUMERICAL RESULTS AND DISCUSSION

The present numerical calculations are those for the case with a flow parallel to the plate where $m = 0$, and Pr and Sc are both equal to unity. The dimensionless plate thickness is fixed at $L^* = 0.03$. The other parameters are changed in the following ranges: $500 \leqslant Re_L \leqslant 50000$; $1 \leqslant R_w \leqslant 50000$; $0.01 \leqslant Bi \leqslant 5000$; $0.1 \leqslant A \leqslant 4$; $-50 \leqslant H \leqslant 50$.

As both Pr and Sc are unity in the present calculations, equations (63) and (64) can be modified respectively as follows:

for the constant-wall-temperature case

$$Nu_x/\sqrt{(Re_x)} = 0.332; \quad (65)$$

for the case with constant interfacial heat flux

$$Nu_x/\sqrt{(Re_x)} = 0.453. \quad (66)$$

Analogous relations for the mass transfer are given as follows:

for the constant-wall-concentration case

$$Sh_x/\sqrt{(Re_x)} = 0.332; \quad (67)$$

for the case with constant interfacial mass flux

$$Sh_x/\sqrt{(Re_x)} = 0.453. \quad (68)$$

The above relations, equations (65) and (67), are represented by a broken line in the following graphs of local Nusselt number and local Sherwood number.

Figure 2 shows the interfacial temperature distributions for various values of Re_L. The other parameters are $Bi = 1000$, $H = 10$, $R_w = 100$, and $A = 0.4$. The value of Bi corresponds to a situation with constant temperature on the opposite plate surface, because the effect of the outer convection is negligibly small.

The interfacial temperature for all values of Re_L is negative in the whole range of x^*, implying that the vaporization markedly lowers the interfacial temperature. It is found that the energy for the vaporization is supplied not only from the gas stream but from the ambient fluid through the flat plate, and that the interfacial temperature decreases with an increase in Re_L. In a simple problem with pure heat transfer,

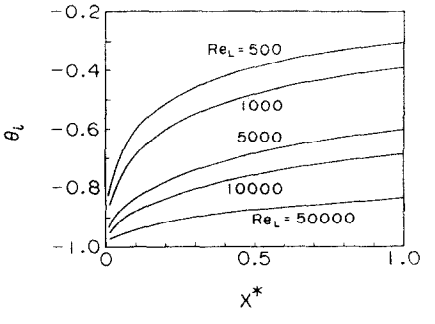

FIG. 2. Interfacial temperature distributions ($Bi = 1000$, $H = 10$, $R_w = 100$, $A = 0.4$, $Pr = Sc = 1.0$, $L^* = 0.03$).

an increase in Re_L enhances the transfer rate between the stream and the plate, as in a simple mass transfer problem. An increase in Re_L prompts both heat and mass transfer rates, but the mass transfer from the surface lowers the interfacial temperature. Thus an increase in Re_L leads to two opposing effects on the temperature field, namely, a rise in the interfacial temperature due to the improvement of heat transfer from the bulk stream to the plate, and a decrease in the interfacial temperature due to enhanced vaporization. The change in the interfacial temperature resulting from an increase in Re_L is determined by the interaction of these effects through the equilibrium relationship.

In Fig. 3, two graphs show the local Nusselt number and Sherwood number in the form of $Nu_x/\sqrt{(Re_x)}$ and $Sh_x/\sqrt{(Re_x)}$, respectively, under the same conditions as in Fig. 2. In the whole x^* region, the curves of $Nu_x/\sqrt{(Re_x)}$ are lower than predicted by equation (65), and the curve for $Re_L = 500$ is the lowest and has the most abrupt decrease in the small x^* region. Such a tendency in the curve is caused by the marked rise in interfacial temperature along x^*. Generally the Nusselt number increases with Re_L because of the enhanced heat transfer.

The curves of $Sh_x/\sqrt{(Re_x)}$ in Fig. 3 are about 5–15% higher than the analogous relation of equation (67). Those at $Re_L = 500$ and 1000 have a maximum near the leading edge. The curve at $Re_L = 50\,000$ is the closest to equation (67) and the change with x^* is small and monotonic.

Figures 4 and 5 show the dependencies of the interfacial temperature, $Nu_x/\sqrt{(Re_x)}$ and $Sh_x/\sqrt{(Re_x)}$ on the opposite side convective heat transfer. In these figures, the Biot number is varied while keeping

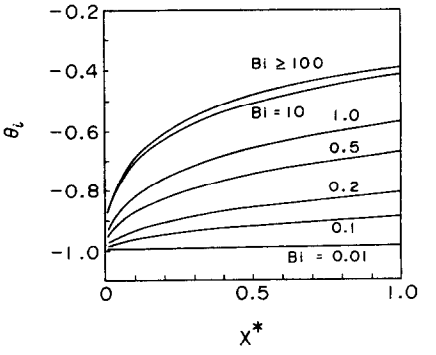

FIG. 4. Interfacial temperature distributions ($Re_L = 1000$, $H = 10$, $R_w = 100$, $A = 0.4$, $Pr = Sc = 1.0$, $L^* = 0.03$).

$Re_L = 1000$ and the other parameters are the same as those for Figs. 2 and 3.

When Bi is small, the interfacial temperature is low, and inversely $Nu_x/\sqrt{(Re_x)}$ is high and close to equation (65). On the other hand, $Sh_x/\sqrt{(Re_x)}$ gets lower with a decrease in Bi and also approaches the analogous relation, equation (67). For $Bi \geqslant 100$ the interfacial temperature loses its dependency on Bi, therefore it can be approximated as a case with constant temperature on the opposite plate surface. Furthermore, as Bi decreases, heat transfer resistance in the ambient fluid becomes dominant in the heat transfer process. Finally the outside boundary condition approaches almost adiabatic as Bi becomes less than 0.01. Under this extreme condition, heat and mass transfers take place in such a way that they are balanced well with each other during the development of boundary layers along the plate. In the present case

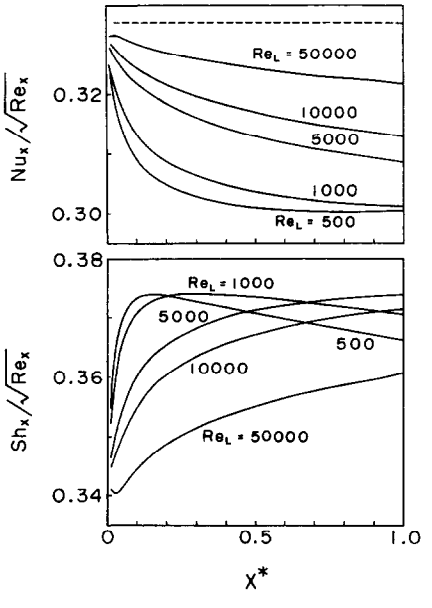

FIG. 3. Distributions of local Nusselt and local Sherwood numbers (broken line, equation (65); $Bi = 1000$, $H = 10$, $R_w = 100$, $A = 0.4$, $Pr = Sc = 1.0$, $L^* = 0.03$).

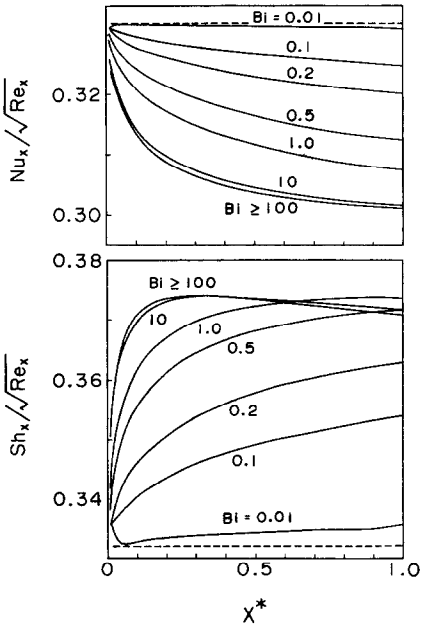

FIG. 5. Distributions of local Nusselt and local Sherwood numbers (broken line, equation (65) or (67); $Re_L = 1000$, $H = 10$, $R_w = 100$, $A = 0.4$, $Pr = Sc = 1.0$, $L^* = 0.03$).

of $Pr = Sc = 1$, where the plate is almost thermally insulated from the ambient, each boundary layer develops along the plate in exactly the same manner. Consequently at $Bi = 0.01$ the interfacial temperature distribution is flat and uniform in the whole range of x^*, which leads to a uniform distribution of interfacial concentration. In this case the interfacial temperature can be estimated by the solutions of two separate problems on heat and mass transfers, by balancing the heat flux and the latent heat of vaporization corresponding to the mass flux at the interface.

For various values of R_w, which is the measure of the wall conductance, distributions of the interfacial temperature, $Nu_x/\sqrt{(Re_x)}$ and $Sh_x/\sqrt{(Re_x)}$ are shown in Figs. 6 and 7. The other parameters are as follows: $Re_L = 5000$, $Bi = 1000$, $H = 10$ and $A = 0.4$. The interfacial temperature is higher at a larger R_w, and the curve at $R_w = 50\,000$ is practically equal to zero, which is the outer plate surface temperature. Concerning $Nu_x/\sqrt{(Re_x)}$ and $Sh_x/\sqrt{(Re_x)}$, the following characteristic behaviors are observed: $Nu_x/\sqrt{(Re_x)}$ between about $x^* = 0.2$ and 0.8 is the smallest at about $R_w = 500$, and $Sh_x/\sqrt{(Re_x)}$ between about $x^* = 0.15$ and 0.75 is the largest at about $R_w = 200$; and for two extremes of R_w, 1.0 and 50 000, the results almost agree with 0.332. The other aspect in the distribution differences from the previous figures, is that some of the curves, for example, the $Sh_x/\sqrt{(Re_x)}$ distribution at $R_w = 1000$, show a change which is not monotonic and has a steep rise and fall along the x^*-axis.

In Figs. 8 and 9, the distributions of the interfacial

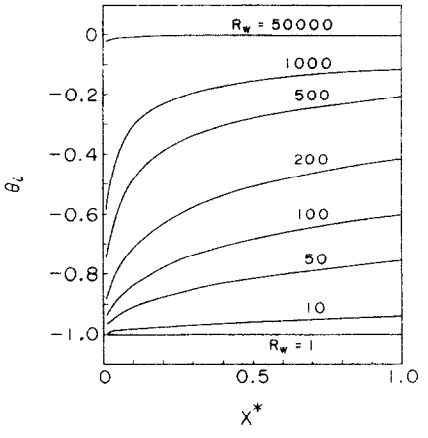

FIG. 6. Interfacial temperature distributions ($Re_L = 5000$, $Bi = 1000$, $H = 10$, $A = 0.4$, $Pr = Sc = 1.0$, $L^* = 0.03$).

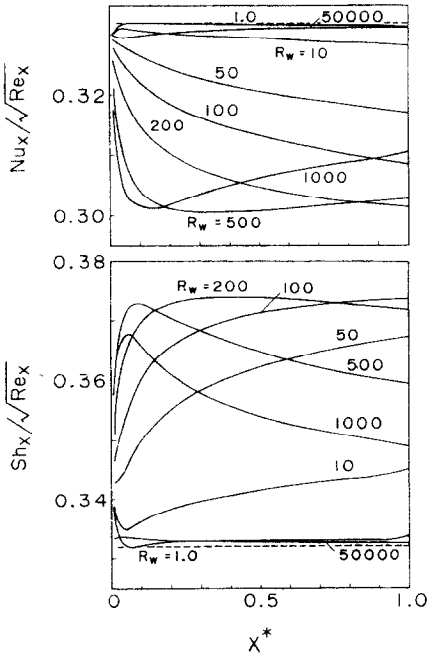

FIG. 7. Distributions of local Nusselt and local Sherwood numbers (broken line, equation (65) or (67); $Re_L = 5000$, $Bi = 1000$, $H = 10$, $A = 0.4$, $Pr = Sc = 1.0$, $L^* = 0.03$).

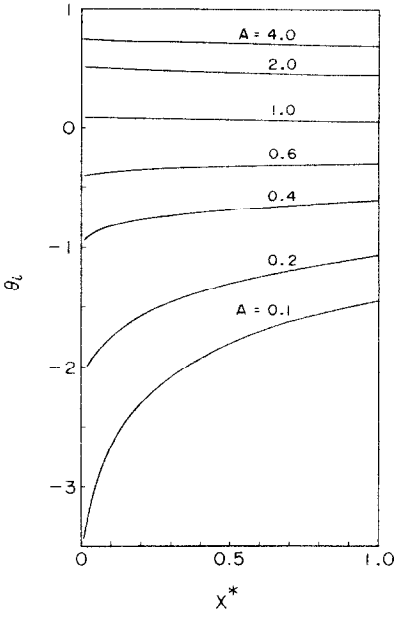

FIG. 8. Interfacial temperature distributions ($Re_L = 5000$, $Bi = 1000$, $H = 10$, $R_w = 100$, $Pr = Sc = 1.0$, $L^* = 0.03$).

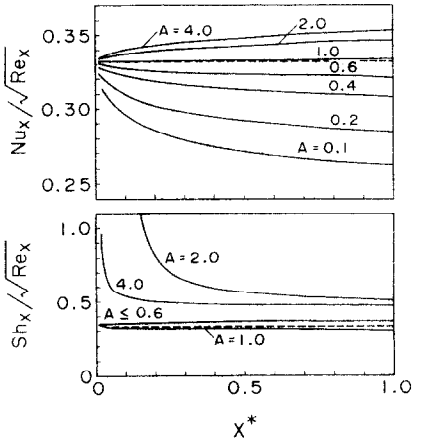

FIG. 9. Distributions of local Nusselt and local Sherwood numbers (broken line, equation (65) or (67); $Re_L = 5000$, $Bi = 1000$, $H = 10$, $R_w = 100$, $Pr = Sc = 1.0$, $L^* = 0.03$).

temperature, $Nu_x/\sqrt{(Re_x)}$ and $Sh_x/\sqrt{(Re_x)}$, are shown for various values of A which is the measure of the temperature dependency of the equilibrium curve for a given system. The other parameters are fixed at $Re_L = 5000$, $Bi = 1000$, $H = 10$ and $R_w = 100$. The interfacial temperature at a smaller value of A is lower and changes more significantly with x^*. The curve of $Nu_x/\sqrt{(Re_x)}$ for $A = 1$ is roughly represented by equation (65), as shown in Fig. 9. Furthermore, at $A = 2.0$ and 4.0, $Nu_x/\sqrt{(Re_x)}$ is larger than 0.332, being different from the distributions in Fig. 7. The curves of $Sh_x/\sqrt{(Re_x)}$ behave in a manner completely different from those of $Nu_x/\sqrt{(Re_x)}$. That is, for $A \leqslant 0.6$, $Sh_x/\sqrt{(Re_x)}$ does not vary so much with x^*, however, $Sh_x/\sqrt{(Re_x)}$ is the lowest at $A = 1.0$ and the highest at $A = 2.0$.

Hereafter, the influence of the parameter H, which is the dimensionless latent heat of vaporization, on heat and mass transfer characteristics, will be discussed.

For various positive values of H, the interfacial temperature, $Nu_x/\sqrt{(Re_x)}$ and $Sh_x/\sqrt{(Re_x)}$ are shown in Figs. 10 and 11. The situation considered in these figures corresponds to that shown in Fig. 1 where the ambient temperature is lower than that of the bulk stream. Conditions for the numerical calculations are fixed as follows: $Re_L = 5000$, $Bi = 1000$, $R_w = 100$ and $A = 0.4$.

At $H = 0.0$, conjugate heat transfer takes place although only the mass transfer is affected by the heat transfer. In the graph, the interfacial temperature is lower at a higher H, showing that the cooling effect of vaporization is substantial. The mass transfer effect is not appreciable for $H \leqslant 0.01$, because the results agree with each other in the range of $0.01 \leqslant H \leqslant 0.0$. On the other hand, though the interfacial temperature is low at $H = 50$, its thermal driving force, the temperature difference between the bulk flow and the interface, is almost uniform in the whole range of x^*. This means that the mass transfer brings the local Nusselt number distribution close to that for the constant-wall-temperature condition, equation (65). Such a behavior is clearly observed in Fig. 11, where $Nu_x/\sqrt{(Re_x)}$ shows the lowest curve at about $H = 5.0$ and 10, which is less than 0.332 given by Pohlhausen [7]. The curves of $Sh_x/\sqrt{(Re_x)}$ monotonously spread with H over a range around 0.332.

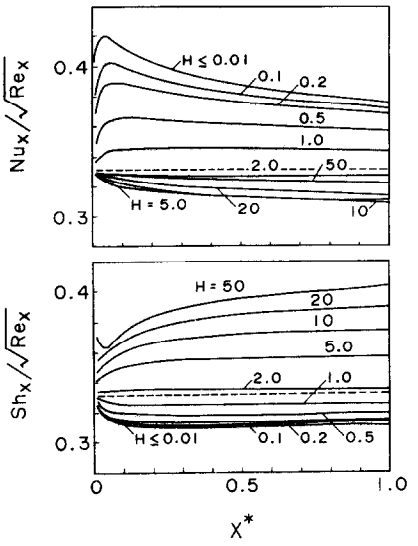

FIG. 11. Distributions of local Nusselt and local Sherwood numbers (positive H; broken line, equation (65) or (67); $Re_L = 5000$, $Bi = 1000$, $R_w = 100$, $A = 0.4$, $Pr = Sc = 1.0$, $L^* = 0.03$).

Figures 12 and 13 show the results for negative values of H. The situation considered in these figures corresponds to the case where the ambient temperature is higher than that of the bulk stream. The conditions for numerical calculations are specified as $Re_L = 5000$, $Bi = 1000$, $R_w = 100$ and $A = -0.4$. The curve of $Nu_x/\sqrt{(Re_x)}$ at $H = -50$, not shown in the upper graph of Fig. 13, almost agrees with that of $H = -20$. The interfacial temperature at $H = -50$ is the highest, however, the driving force for heat trans-

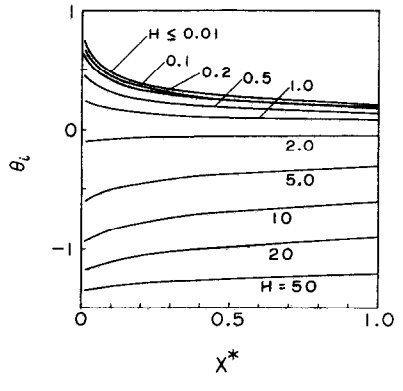

FIG. 10. Interfacial temperature distributions (positive H; $Re_L = 5000$, $Bi = 1000$, $R_w = 100$, $A = 0.4$, $Pr = Sc = 1.0$, $L^* = 0.03$).

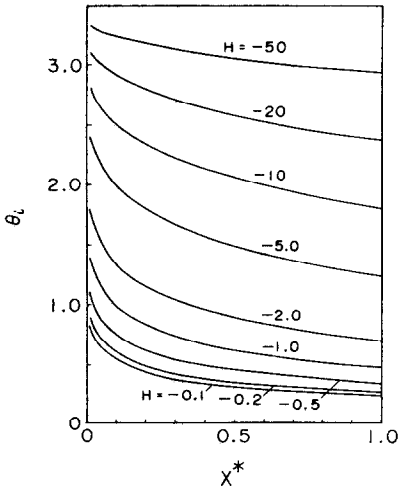

FIG. 12. Interfacial temperature distributions (negative H; $Re_L = 5000$, $Bi = 1000$, $R_w = 100$, $A = -0.4$, $Pr = Sc = 1.0$, $L^* = 0.03$).

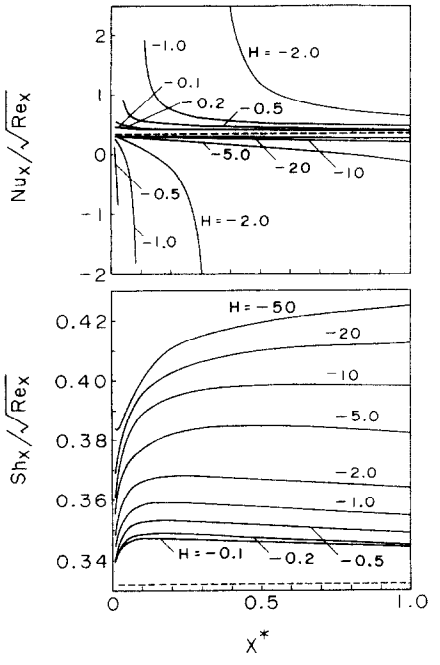

FIG. 13. Distributions of local Nusselt and local Sherwood numbers (negative H; broken line, equation (65) or (67); $Re_L = 5000$, $Bi = 1000$, $R_w = 100$, $A = -0.4$, $Pr = Sc = 1.0$, $L^* = 0.03$).

fer is less dependent on x^* in comparison with those for the other values of H. This small change in the temperature difference along the x^*-axis gives the local Nusselt number distribution close to equation (65), as shown in the upper graph of Fig. 13. Appearance of a discontinuous point is notable in the $Nu_x/\sqrt{(Re_x)}$ distribution for $-0.5 \geqslant H \geqslant -2.0$. On the other hand, $Sh_x/\sqrt{(Re_x)}$ is higher at a lower H, without any higher or lower limit of influence.

Further discussion will be made below, based on all of the above numerical results.

According to the previous study on pure heat transfer with boundary layer flow with thermal conjugation between the flow and the plate wall [4], the interfacial temperature settles down between $\theta = 0$ and 1 (the temperatures of the ambient and bulk stream, respectively) due to the thermal interaction. The resulting distribution of the local Nusselt number has an intermediate curve between equation (66) as the upper limit for the constant-wall-heat-flux case and equation (65) as the lower limit for the constant-wall-temperature case. Generally the local Nusselt number rises with an increase in the thermal driving force with x^*, i.e. an increase in the temperature difference between the interface and the bulk stream.

In the present problem, the interfacial temperature varies in a range much wider than $0 \leqslant \theta \leqslant 1$, and the local Nusselt number and local Sherwood number also change beyond the two limiting values for the constant-wall-heat-flux and constant-wall-temperature cases, as mentioned above. Furthermore, the distribution of the Nusselt number has a discontinuous point occasionally as in the upper graph of Fig. 13, and probably the distribution of the Sherwood number as well, as suggested in the lower graph of Fig. 9. Thus the interaction between mass transfer to the boundary layer flow and conjugate heat transfer with the flow and the plate wall, is not straightforward, and this effect is hard to estimate properly from the solutions of the simplest heat transfer problems treated by Pohlhausen and Kays and those for mass transfer derived analogously from the heat transfer. The present comprehensive analysis becomes significant and effective in order to obtain theoretical prediction, especially for cases where the vapor–liquid equilibrium is highly temperature dependent and/or latent heat of vaporization is large.

Appearance of a discontinuity in the distribution of the local Nusselt number can be explained as follows. As an example of such a case, the results at $H = -2.0$ shown in Figs. 12 and 13 will be considered. The interfacial temperature gradually decreases along the x^*-axis and cuts across the line of $\theta_i = 1.0$ at $x^* = 0.37$. This means that the superficial driving force of the heat transfer changes from negative to positive at the intersection. On the other hand, in the vicinity of the leading edge, the local heat flux is in the direction from the interface to the bulk stream and changes its direction downstream. But the change in the heat-flux direction does not synchronize with a decrease in the apparent driving force. This mismatch causes a discontinuity in the local Nusselt number distribution. In the case of mass transfer also, the appearance of a discontinuity in the local Sherwood number could be explained in a similar manner.

4. CONCLUSION

Theoretical analysis has been conducted for evaporation to a laminar boundary layer flow from a flat plate surface, where the convective heat and mass transfers and the two-dimensional thermal conduction in the plate are combined simultaneously. The conjugation is achieved by taking into account the vapor–liquid equilibrium of linear temperature dependence at the interface, the latent heat of vaporization and the continuities of temperature and heat flux at the interface. Convective heat transfer described by a constant heat transfer coefficient is assumed in the ambient fluid.

Numerical calculations have been made for the parallel flow case where both values of the Prandtl and Schmidt numbers are unity. Based on distributions of the interfacial temperature, $Nu_x/\sqrt{(Re_x)}$ and $Sh_x/\sqrt{(Re_x)}$ obtained, the interaction of heat and mass transfers and the effect of wall conduction on it are discussed and the following conclusions are derived.

The interfacial temperature varies in a wide range; from a value much lower than the ambient temperature, $\theta = 0$, to that higher than the bulk stream tem-

perature, $\theta = 1$. The local Nusselt number also changes beyond the lower and upper limits for pure conjugate heat transfer for the cases with the constant temperature and constant heat flux on the outer plate surface. Furthermore, a discontinuity occasionally appears in the Nusselt number distribution.

The local Sherwood number also shows such behavior as that of the local Nusselt number, however, both behaviors are not analogous even when the Prandtl and Schmidt numbers have the same value.

In general, the characteristics in heat and mass transfers are highly conjugated with each other and significantly influenced by the temperature dependency of the vapor–liquid equilibrium, the magnitude of the latent heat of the phase change and the thermal conductance of the flat plate. Only in a few cases with a very small Biot number or extremely large thermal conductance of the plate, can the situation be properly predicted from the solutions of the simplest heat transfer problems as treated by Pohlhausen and that for mass transfer derived analogously from the heat transfer analyses.

Acknowledgement—All the numerical calculations were performed by using a computer of Kanazawa University Information Processing Center.

REFERENCES

1. S. Kikkawa and K. Yoshikawa, Theoretical investigation on laminar boundary layer with combustion on a flat plate, *Int. J. Heat Mass Transfer* **16**, 1215–1229 (1973).
2. T. L. Perelman, On conjugated problems of heat transfer, *Int. J. Heat Mass Transfer* **3**, 293–303 (1961).
3. A. V. Luikov, T. L. Perelman, R. S. Levitin and L. B. Gdalevich, Heat transfer from a plate in a compressible gas flow, *Int. J. Heat Mass Transfer* **13**, 1261–1270 (1970).
4. M. Sakakibara, S. Mori and A. Tanimoto, Effect of wall conduction on convective heat transfer with laminar boundary layer, *Heat Transfer—Jap. Res.* **2**, 94–103 (1973).
5. A. V. Luikov, Conjugate convective heat transfer problems, *Int. J. Heat Mass Transfer* **17**, 257–265 (1974).
6. A. Pozzi and M. Lupo, The coupling of conduction with forced convection over a flat plate, *Int. J. Heat Mass Transfer* **32**, 1207–1214 (1989).
7. E. Pohlhausen, Wärmeaustausch zwischen festen Körpen und Flüssigkeiten mit kleiner Reibung und kleiner Wärmeleitung, *Z. Angew. Math. Mech.* **1**, 115 (1921).
8. W. M. Kays and M. E. Crawford, *Convective Heat and Mass Transfer*, 2nd Edn, p. 151. McGraw-Hill, New York (1980).

TRANSFERT DE CHALEUR ET DE MASSE POUR UN ECOULEMENT A COUCHE LIMITE SUR UNE PLAQUE PLANE D'EPAISSEUR FINIE

Résumé—On analyse théoriquement l'évaporation à partir d'une surface de plaque plane pour un écoulement à couche limite laminaire en prenant en compte la conduction thermique bidimentionnelle dans la plaque avec une condition limite thermique de convection sur l'autre face de la plaque. L'effet thermique de la volatilité du liquide sur la plaque est négligé. Des distributions de température interfaciale et de nombre de Nusselt et de Sherwood locaux sont calculées pour un écoulement parallèle ayant des nombres de Prandtl et de Schmidt égaux à l'unité. Les caractéristiques du transfert de chaleur et de masse sont significativement influencées par la dépendance vis-à-vis de la température de l'équilibre liquide–vapeur, l'importance de la chaleur latente de changement d'état et la conductance thermique de la plaque plane.

WÄRME- UND STOFFÜBERTRAGUNG IN EINER GRENZSCHICHTSTRÖMUNG ÜBER EINE EBENE PLATTE ENDLICHER DICKE

Zusammenfassung—Die Verdampfung von der Oberfläche einer ebenen Platte in eine laminare Grenzschichtströmung längs der Platte wird theoretisch untersucht. Dabei wird die zweidimensionale Wärmeleitung in der Platte, und die konvektive Randbedingung an der anderen Plattenoberfläche berücksichtigt. Einflüsse, die sich möglicherweise bei der Zufuhr der verdampfbaren Flüssigkeit ergeben, werden vernachlässigt. Für eine parallele Strömung, bei der sowohl die Prandtl-Zahl als auch die Schmidt-Zahl gleich eins ist, werden die Verteilungen der Grenzflächentemperatur sowie der örtlichen Nusselt- und Sherwood-Zahl berechnet. Das Verhalten des Wärme- und Stoffübergangs wird wesentlich von der Temperaturabhängigkeit des Dampf-/Flüssigkeitsgleichgewichts, von der Größe der Verdampfungsenthalpie und von der Wärmeleitfähigkeit der ebenen Platte beeinflußt.

ТЕПЛО- И МАССОПЕРЕНОС В ПОГРАНИЧНОМ СЛОЕ НА ПЛОСКОЙ ПЛАСТИНЕ КОНЕЧНОЙ ТОЛЩИНЫ

Аннотация—Теоретически анализируется тепло- и массоперенос при испарении в ламинарном пограничном слое на плоской пластине с учетом двумерной теплопроводности в пластине и граничного условия 3-го рода на другой поверхности. Тепловой эффект подвода летучей жидкости к пластине не принимается во внимание. Рассчитываются распределение температур на границе раздела, а также локальные числа Нуссельта и Шервуда в случае, когда числа Прандтля и Шмидта равны единице. Показано, что на характеристики тепло- и массопереноса значительное влияние оказывает зависимость давления насыщенных паров от температуры, величина скрытой теплоты фазового превращения, а также теплопроводность плоской пластины.